Journal of Fluorescence (2024) 34:587–598
https://doi.org/10.1007/s10895-023-03290-4

RESEARCH

Synthesis, Spectroscopic, and Antibacterial Characterizations of Cadmium–Based Nanoparticles

J. Christina Rhoda[1] · S. Chellammal[1] · Helen Merina Albert[2] · K. Ravichandran[3] · C. Alosious Gonsago[4]

Received: 17 May 2023 / Accepted: 27 May 2023 / Published online: 16 June 2023

Abstract

In the current study, the co-precipitation technique was employed for the synthesis of Cadmium oxide (CdO) and Copper−doped Cadmium oxide (Cu−CdO) nanoparticles. The synthesized samples were subjected to powder X-Ray diffraction (P-XRD), Field emission scanning electron microscopy (FE-SEM), Energy-dispersive X-ray (EDX), Fourier transforms Infrared (FT-IR), UV–Vis spectroscopy, photoluminescence (PL), laser-induced fluorescence spectroscopy and antibacterial investigations. According to the P-XRD analysis, both the samples were simple cubic in structure and have average grain sizes of 54 and 28 nm, respectively. FE-SEM was deployed to explore the surface textures of the samples. EDX technique was used to look at the elemental compositions of the samples. The technique of FT-IR was employed to identify the vibrational modes. UV–Vis spectra in diffuse reflectance mode were obtained and the optical bandgaps of the CdO and Cu−CdO samples were obtained as 4.52 eV and 2.83 eV, respectively. The photoluminescence studies were conducted at an excitation wavelength of 300 nm and emission peaks were red-shifted in both samples. Fluorescence spectroscopy was applied to explore the lifetimes of synthesized nanoparticles. The technique of Agar-well diffusion was applied to assess the antibacterial performance of the generated nanoparticles against *Micrococcus Luteus* (gram-positive) and *Escherichia coli* (gram-negative) bacterium at variable concentrations. Both samples in the current study are significantly effective against both bacterial strains.

Keywords XRD · FE-SEM · EDX · UV–visible · Fluorescence · Antibacterial Effect

Introduction

Nanotechnology is about the investigation and redesign of matter between one and 100 (nm) in dimension, where these materials' physical and chemical properties will be entirely different from those of their bulk form. Nanoparticles display a wide variety of chemical and physical features due to their reduced size, including colloidal attributes, optical, electrical, and magnetic characteristics [1–3]. Given their numerous applications in semiconductor materials, sensors, optoelectronic devices, photonics, computing, and biological domains, nanoparticles have been receiving a lot of attention [4–6]. The development and analysis of metal-oxide nanostructures are useful for both identifying basic phenomena in low-dimensional system applications and designing novel high-performance nano-devices. Nano-sized semiconductor metal oxides are also a focus of research in the sector of energy generation because of their optical and electrical characteristics [7]. The metal oxide semiconducting material CdO has received a lot of attention in recent years due to its uses in many fields of study, particularly optoelectronic

✉ C. Alosious Gonsago
c.alosious@gmail.com

J. Christina Rhoda
j.christinarhoda@yahoo.com

S. Chellammal
selvi.chella@yahoo.co.in

Helen Merina Albert
drhelenphy@gmail.com

K. Ravichandran
ravi_21068@yahoo.com

[1] Department of Physics, Dr. M.G.R. Educational & Research Institute, Chennai, India

[2] Department of Physics, Sathyabama Institute of Science & Technology, Chennai, India

[3] Department of Nuclear Physics, University of Madras (Guindy Campus), Chennai, India

[4] Department of Electronics Science, Mohamed Sathak College of Arts & Science, Chennai, India

devices, such as solar cells, photodiodes, phototransistors, transparent electrodes, gas sensors, etc. [8–10]. An n-type oxide of the II-VI group, cadmium oxide (CdO) is found naturally in the red monteponite or rare mineral brown single crystals.

Nano-scaled CdO is an excellent contender for a variety of technical applications in numerous domains due to its ionic nature, minimal resistance, high carrier mobility, and adequate optical transmission in the visible region. The CdO nanoparticles have interesting fluorescence properties, and their performance is higher than that of organic dyes [11]. A fluorescence lifespan is the period of time a fluorophore remains in the stimulated state before reverting to its fundamental state and emitting a photon [12]. A lifetime of a fluorophore could be determined by time-resolved fluorescence spectroscopy [13]. Non-radiative decay dominates the fluorophore's relaxation process when the energy gap across the bottom and energized states narrows down. Therefore, the quantity of information received from organic-based fluorophores is insufficient, and they lack the optical properties required for substantial fluorescent signals. An alternative strategy to circumvent these limitations associated with organic fluorophores is to employ inorganic semiconductor nanoparticles. The lifetime, extinction coefficients, and quantum yield of these particles are tunable using the size, morphology, and bandgap of synthesized nanoparticles [14].

Many scholars have conducted substantial research on CdO nanoparticles prepared through many synthesis techniques, including microwave combustion and co-precipitation methods [15–19]. The synthesis of a significant amount of metal oxide nanostructures in a variety of shapes has also been accomplished using the microwave combustion technique. In this approach, the microwave energy directly interacts with the dipoles found in the reaction mixtures to produce energy-efficient internal heating [16]. The co-precipitation method is an effective soft chemical process for synthesizing inorganic and metal-based nanoparticles, which is frequently referred to as the solid-state equivalent of the sol–gel process. With easily available precursors, the co-precipitation approach provides a simple and cost-effective synthesis strategy in this investigation. This approach provides a number of benefits, including a high yield of products, an eco-friendly solvent, and extremely narrow size dispersion. In the present investigation, CdO and Cu−CdO nanoparticles were produced by the co-precipitation process. The crystal structure, surface morphology, elemental composition, optical spectroscopy, and influence of copper doping on the antibacterial ability of CdO nanoparticles are all detailed. The synthesized CdO nanomaterials may be implemented as an alternative to conventional antibiotics since they are more resistant to pathogenic microbes. The CdO nanomaterials synthesized by the co-precipitation techniques are predicted to have a variety of properties; thus, their antibacterial impact is critical. Finding a low-cost effective method for inhibiting pathogenic bacteria's growth and activity is essential given how challenging it is for most people to deal with the rising costs of curing them. One of the compatible approaches for testing produced nanoparticles against various types of bacteria is the agar well method. Many researchers have used this method in their approach [20–22]. The pathogenic microorganisms have been confronted with CdO nanoparticles. The influence of doping copper to CdO nanoparticles on their antibacterial effectiveness against pathogenic pathogens such as *Micrococcus Luteus* and *Escherichia Coli* are discussed in detail in this research.

Experimental

Briefly, the co-precipitation process entails first dissolving the starting chemicals in a general solvent and then a precipitating agent is added in order to produce a homogenous and single-phase inorganic substance. The target material oxide can then be synthesized by decomposing the precipitate at an elevated temperature. Co-precipitation decreases the decomposition temperature and aids in keeping the necessary cations together in the reaction media. In our case, CdO and Cu–CdO nanoparticles were produced using analytical reagent grades of Cadmium Chloride ($CdCl_2$), Sodium Hydroxide (NaOH), and Copper Chloride ($CuCl_2$) by employing the co-precipitation technique at 30 °C. For the synthesis of CdO nanoparticles, the required amount of cadmium chloride was first dissolved in 100 ml of deionized water and thoroughly stirred for 1 h to form a homogenous cadmium hydroxyl solution. Drop by drop, sodium hydroxide solution (precipitating agent) was introduced into the cadmium hydroxyl solution, and the pH of the solution was set to 8. A milky white solution was formed after four hours of continuous stirring. The precipitate was cleaned in methanol, which was then left to evaporate at room temperature to produce white powdered cadmium hydroxide. The cadmium hydroxide particles were then added to a hot-air oven, which had been heated to 300 °C. After four hours, the cadmium oxide powders were obtained for further use. The Cu–CdO nanoparticles were obtained by adding 0.05 mol% $CuCl_2$ to the Cadmium Hydroxyl solution and by following the above same synthesis procedure. The synthesis process is depicted schematically in Fig. 1. The following was the reaction:

$$CdCl_2 + 2NaOH \rightarrow Cd(OH)_2 + 2NaCl$$

$$Cd(OH)_2 \rightarrow CdO + H_2O$$

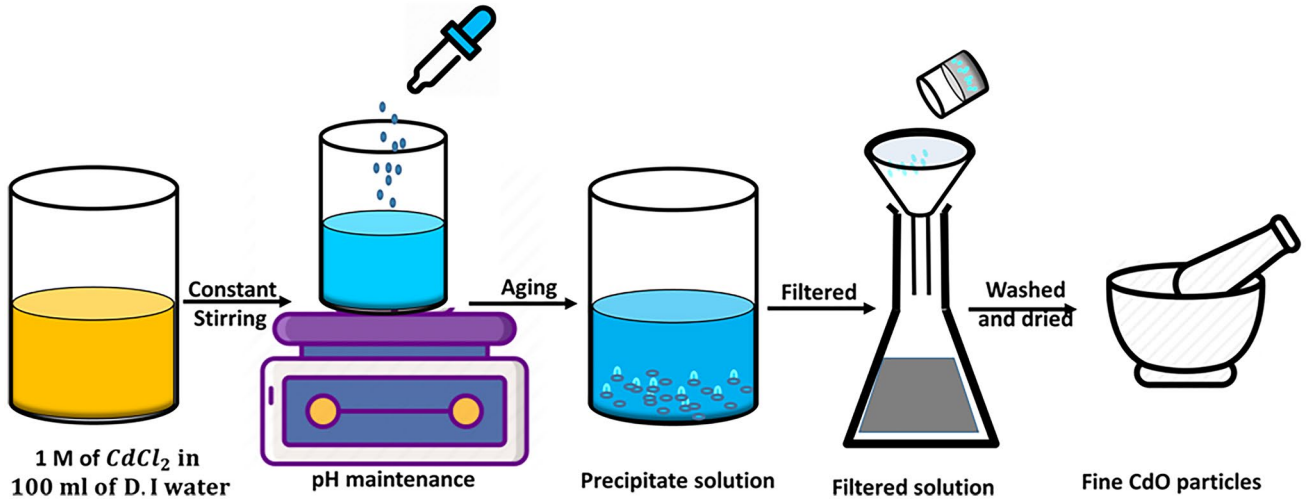

Fig. 1 Schematic of the synthesis of CdO nanoparticles

Characterization Techniques

In order to provide insight into the structural phase of the created nanoparticles, P-XRD measurements were performed on the produced samples using a D8-Advance-Bruker diffractometer. By employing an FE-SEM analyzer (FEI Quanta-FEG:200), the surface textures of the generated particles were investigated. It also presents crystalline information through the EDX quantification through an electron backscattered detection (BSD) system attached to a microscope. FT-IR spectroscopic measurements were carried out using a Perkin-Elmer spectrometer between 4000–400 cm^{-1} ranges. UV–Vis measurements were performed using an Ocean-Optics USB4000 UV–Vis spectrophotometer to record the absorption spectra in reflectance mode (DRS). PL studies were conducted with Perkin-Elmer spectrophotometer L.S-45 in the range of 200–900 nm. Jobin–Yvon M/S time-resolved fluorescence observations were performed with a pulsed laser excitation source and a fast response PMT detector using a time-correlated single-photon counting (TCSPC) method. The technique of diffusion on agar wells was implemented to test the antibacterial effects of the produced nanoparticles against the gram-negative bacterium (*Escherichia Coli*) and gram-positive bacteria (*Micrococcus Luteus*).

Results and Discussion

Powder-XRD Investigation

Powder XRD is a prominent method for determining crystal structure at the atomic level. It is a non-destructive technique with a lot of prospective for characterizing both bulk and nanomaterials [23]. The XRD patterns of the as-synthesized CdO and Cu–CdO nanoparticles are depicted in Fig. 2. Prominent and intensive diffraction peaks can be seen in XRD patterns and match with the simple cubic phase of CdO (JCPDS Card No: 78–1125). The XRD pattern of as-prepared CdO shows prominent peaks at (111), (200), (101), (210), (220), (211), and (310) planes that are concurrent with the reported data [24]. In addition to these peaks, the XRD pattern also displays a number of other small peaks that were not assigned. These additional peaks are believed to have occurred as a result of the nanparticle's phase coagulation. The samples are of good crystallinity, as observed in the diffractogram. The addition of the dopant did not change the composition of nanoparticles. The typical grain size of the CdO and Cu–CdO were determined from the subsequent Scherrer equation:

$$\text{Average grain size, } D = \frac{k\lambda}{\beta_{hki}\cos\theta} \tag{1}$$

where, D is the mean size of particles measured in nanoscale, λ is the radiation wavelength, θ is the diffraction angle, β_{hkl} is the full-width at half maximum (FWHM), and k is taken as 0.9.

The XRD plots display that the CdO particles are primarily solidified together with the (111) orientation. The highly intense peaks are considered for estimating the mean size of the nanoparticles using Eq. (1). The diffraction curves of CdO and Cu−CdO nanoparticles, revealed the nanoparticles with average sizes of 54 and 28 nm, respectively. Cu doping in CdO nanoparticles involves replacing some of Cd^{2+} with Cu^{2+} ions in the host CdO lattice, which decreases the particle size in Cu–CdO. The ionic radius of Cu^{2+} is 0.073 nm which is lesser than that of Cd^{2+} (0.097 nm). When Cu^{2+} is

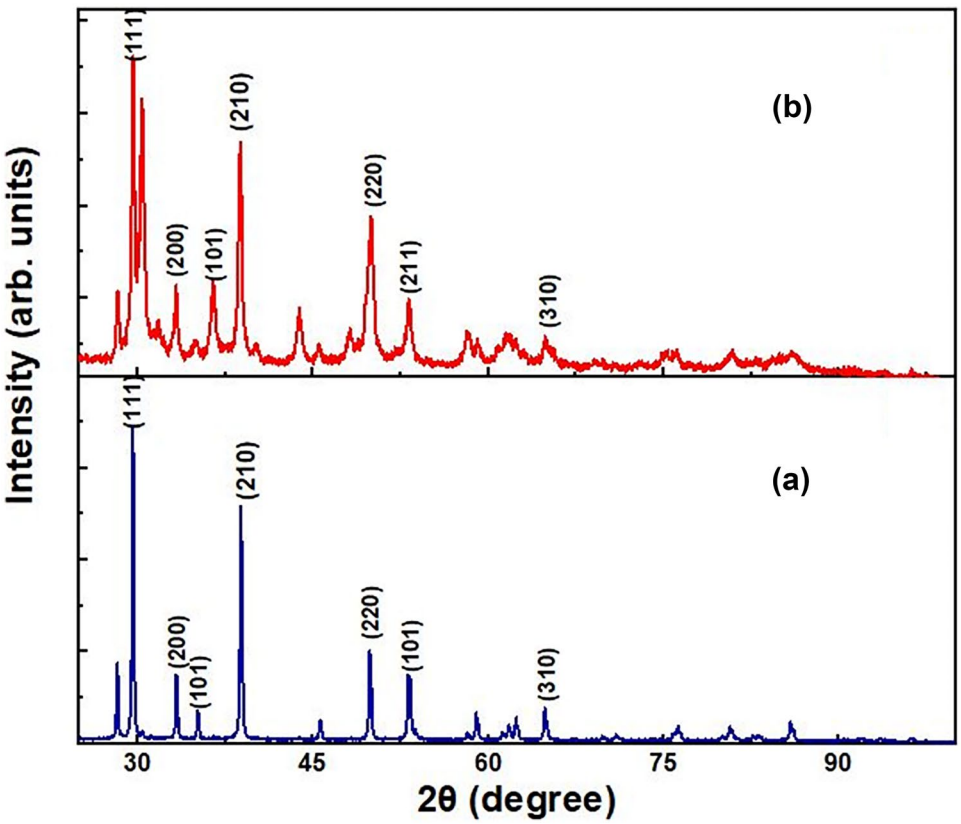

Fig. 2 XRD plots of **a** CdO and **b** Cu–CdO nanoparticles

introduced as a dopant, it substitutes Cd^{2+} with tiny voids in the host lattice. These voids cause a lattice distortion altering the size of Cu−CdO nanoparticles.

FE-SEM and EDX Findings

The FE-SEM imaging mechanism allows for the observation of small structures with dimensions of a few nm or less. The FE-SEM offers high imaging at low accelerating voltages and close working distances. Physicists, chemists, and Biologists employ this technique to find structures up to 1 nm [25, 26]. The FE-SEM imaging was performed to examine the structures of the given nanoparticles and is displayed in Fig. 3. The images demonstrate that the nanoparticles are agglomerated homogeneous structures with well-defined grain boundaries. The structures of these nano samples are almost spherical, and few voids are also observed in between them.

The chemical compositions of as-produced samples were analyzed by EDX spectroscopy [27]. The characteristic peaks associated with Cd, O, and Cu are visible in the spectra of the prepared samples, as shown in Fig. 4, confirming the formation of CdO and Cu–CdO nanoparticles. The outputs related to Cd, O, and Cu substantiate the formation of pure and Cu–CdO nanoparticles. The weight percentages of elements as determined by EDX results are presented in

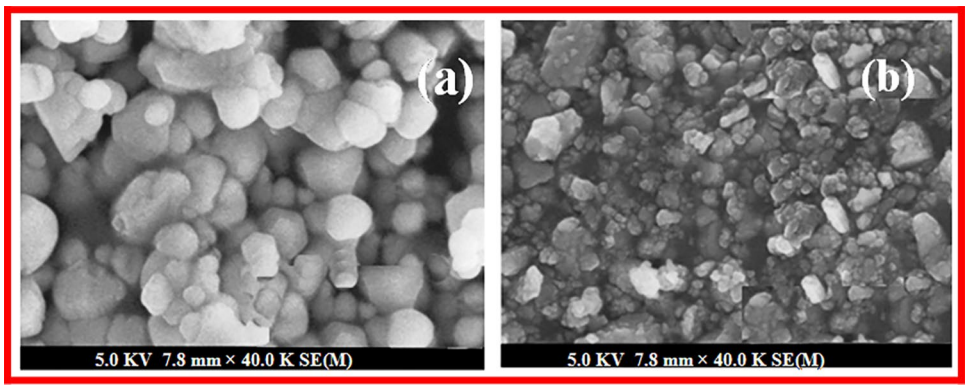

Fig. 3 FE-SEM images of **a** CdO, and **b** Cu–CdO nanoparticles

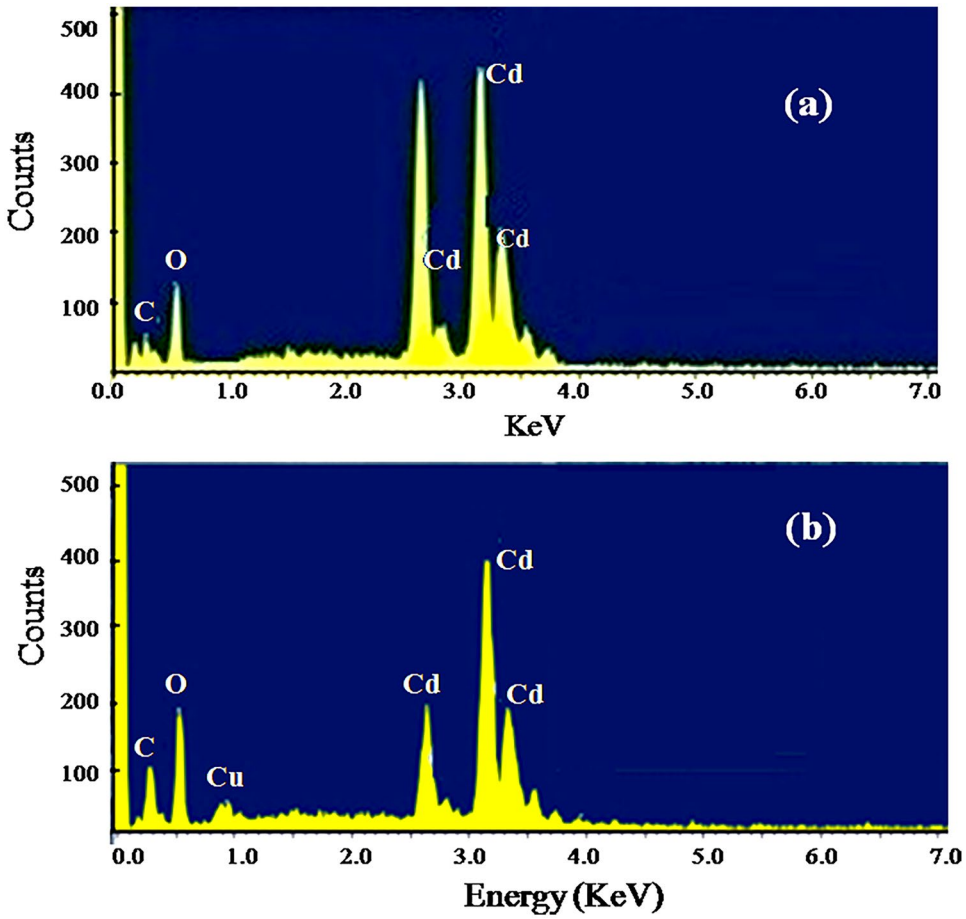

Fig. 4 EDX spectra of **a** CdO and **b** Cu−CdO nanoparticles

Table 1. The availability of carbon, oxygen, cadmium, and copper in the right percentages supports subsequent formulations of CdO and Cu–CdO nanoparticles.

FT-IR Spectroscopy

FT-IR is an incredibly valuable tool for establishing the identity of substances [28, 29]. FT-IR technique has numerous applications, ranging from process monitoring to compound identification to detecting constituents in mixtures. This method centered on identifying functional groups of molecules that oscillate either by bending or stretching in different modes when exposed to certain wavelengths. To generate an FT-IR graph, these oscillations and their level of intensity are displayed against the wavenumber of light (cm^{-1}) under which the specimen is treated. Each compound absorbs light at unique frequencies, and each functional group has characteristic absorption bands. The recorded spectra of the as-synthesized nanoparticles are depicted in Fig. 5. The bands at 3465 and 3444 cm^{-1} are as a result of the stretching of the hydroxyl group in $Cd(OH)_2$. The band associated with C-H asymmetric stretching appears at 2928 and 2925 cm^{-1}. A peak of about 1628 cm^{-1} is associated with the

Table 1 EDX spectroscopic data of CdO, and Cu−doped CdO nanoparticles

Element	CdO (Wt %)	Cu-CdO (Wt %)
C K	2.62	6.46
O K	29.09	36.38
Cd L	68.29	56.72
Cu L	0.0	0.44

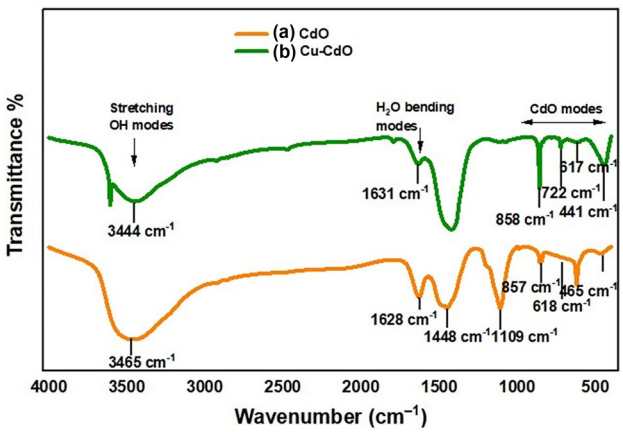

Fig. 5 FT-IR curves of CdO, and Cu–CdO nanoparticles

water molecule's vibrations and is probably caused by water adsorption as a result of KBr compression of the powdery nanoparticles. The peak of about 1448 cm^{-1} is designated to asymmetric stretching of water molecules linked with generated CdO. Absorbance at 857 cm^{-1} is related to the stretching vibrations of the Cd–O bond. The bands at 618, 617, 465, and 441 cm^{-1} indicate the generation of Cd–O. According to the available literature, the intense I.R. peaks at around 500, 1000, and 1400 cm^{-1} are the typical bands of the Cd–O. As a result, we conclude that the precursor nanoparticles formed contain hydroxyl (−OH) and cadmium (Cd^{2+}) ions.

UV–Vis Spectroscopy

The chemical, molecular, and structural features of a material are identified, ascertained, and measured using the UV−Vis Spectroscopy. Different kinds of atomic particles will absorb or emit different amounts of electromagnetic spectrum. This feature allows spectroscopy to determine and assess the nature of the sample [30]. The curves in the diffuse reflectance mode were recorded between 200–1000 nm ranges. Figure 6 depicts the recorded reflectance spectra, whereas Fig. 7 depicts the bandgap of synthesized samples. The Kubelka–Munk function is used to renovate the reflectance statistics into absorbance statistics, as shown in Eq. (2).

$$F(R) = \frac{(1-R)^2}{2R} \tag{2}$$

Where, $F(R)$ represents the Kubelka–Munk function and R represents the reflectance (%). A plot of K-M function $[F(R)h\nu]^n$ *vs* photon energy $h\nu$ gives Tauc's plot, where h is Planck's constant and ν is the frequency of the beam. The optical cut-off edge is detected at 273 nm for the as-prepared samples. Compared to CdO, the absorption edge of Cu−CdO is blue-shifted. The absorbance spectra of CdO exhibit a characteristic cut-off edge of 436 nm, which decreases rapidly at a longer wavelength region. The optical bandgap (E_g) values corresponding to the absorption edges for CdO and Cu−CdO nanoparticles are 4.52 and 2.83 eV, respectively. The bandgap of CdO nanoparticle is larger than that of bulk CdO (2.30 eV), indicating a red shift due to the quantum confinement of the nanoparticles [31].

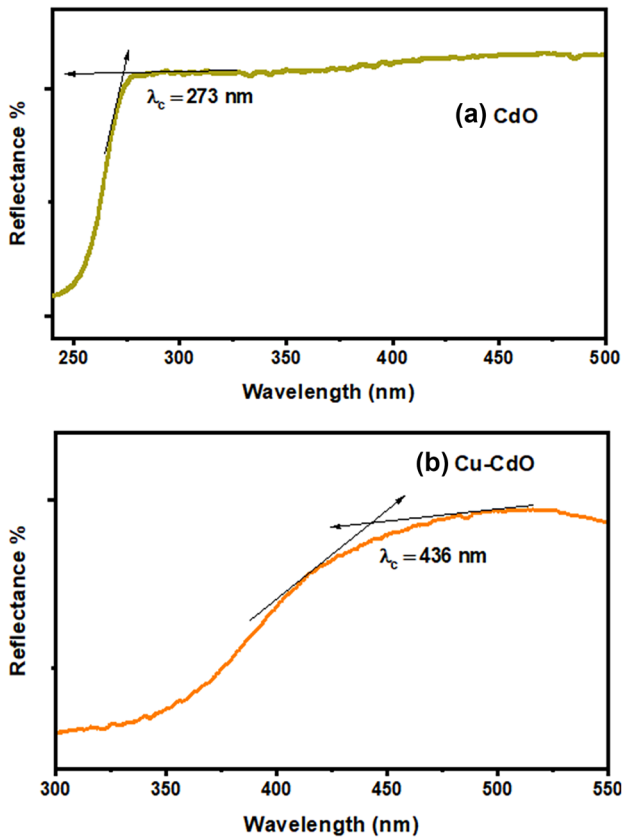

Fig. 6 Reflectance spectra of **a** CdO and **b** Cu–CdO nanoparticles

Photoluminescence Spectroscopy

Photoluminescence spectroscopy (PL) has been used to describe the optical characteristics of semiconductors. It is frequently used to describe complicated molecules, and their positions in molecular biology or biochemistry [32]. In PL spectroscopy, light waves induce the emission of photons from any substance, providing a non-invasive way to examine materials. An optical spectrometer is employed to determine the intensity of the light which is emitted as a function of wavelengths. The PL bands of the synthesized samples were obtained by illuminating CdO nanoparticles at 300 nm, as illustrated in Fig. 8. The spectra show an emission band in the red region (608 nm). The emission peaks might shift as a result of enhanced conjugation in a substance or as a result of molecules grouping together. The broad, intense emission band is owing to oxygen vacancies and cadmium interstitials. Structural perfection and surface defects in the compound contribute to the intensity of emission peaks. Doped–CdO nanoparticles result in a minor variation in peak intensity. The amount of peaks is connected to the crystallinity of the nanoparticles, and the intensity of the nanoparticles is at its highest. Better crystallinity and optimization of chemical composition are some of the requirements for developing efficient materials depending on the required application.

The chromaticity diagram was created by mapping the emitted light intensity from the samples, given in the Fig. 8c and d. The chromaticity coordinates of the CdO sample are x = 0.635 and y = 0.348. The coordinates were calculated based on the tristimulus values using the Eq. (3),

$$x = \frac{x}{x+y+z} \;\&\; y = \frac{y}{x+y+z} \tag{3}$$

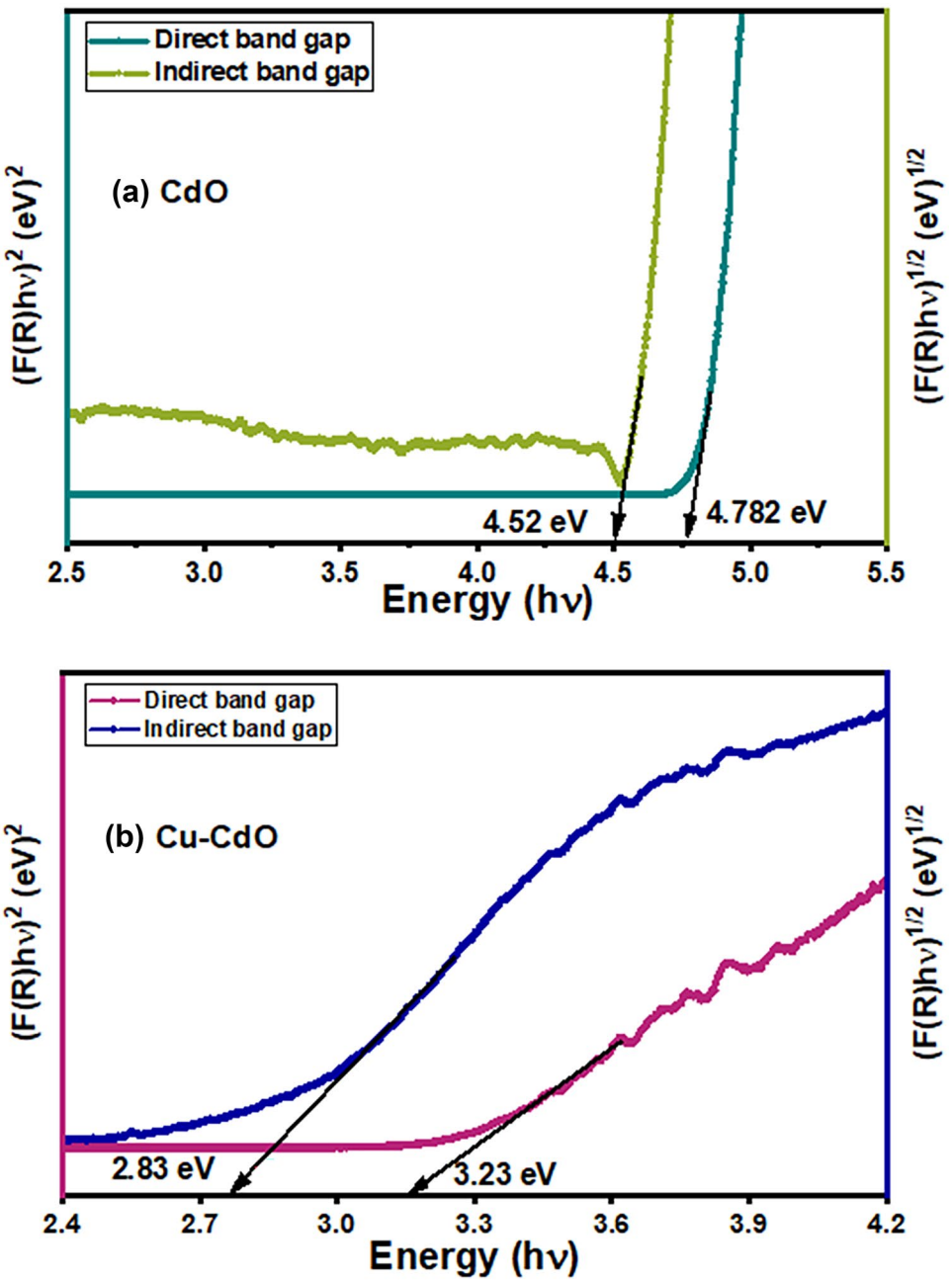

Fig. 7 Bandgaps estimation of **a** CdO, and **b** Cu–CdO nanoparticles

From the chromaticity illustration, red emission is observed for both CdO and Cu–CdO nanoparticles. The outer circumference in the chromaticity diagram is the spectral locus, and the wavelengths are noted in nanometers.

Fluorescence Spectroscopy

Time-correlated single photon counting (TCSPC) method was applied for the lifetime measurements of the particles [33]. The observed data is in the form of a discrete-time function, with the rate of detection being 1 photon for 100 pulsations. The sensitivity of this method is superior to any other since it can detect a very low emission from a sample and measures the emission lifetime [34]. The use of lasers and PMT detectors allows a lifetime measurement of up to a few seconds. The CdO sample was excited with a pulsed laser at 280 nm (λ_{ex}), and decay measurements were made at 339 nm (λ_{em}) based on absorption and emission analyses. If τ is denoted as the lifetime and I_0, the intensity at time $t = 0$, then the exponential decay distribution can be expressed in Eq. (4), referred to as the first-order rate equation:

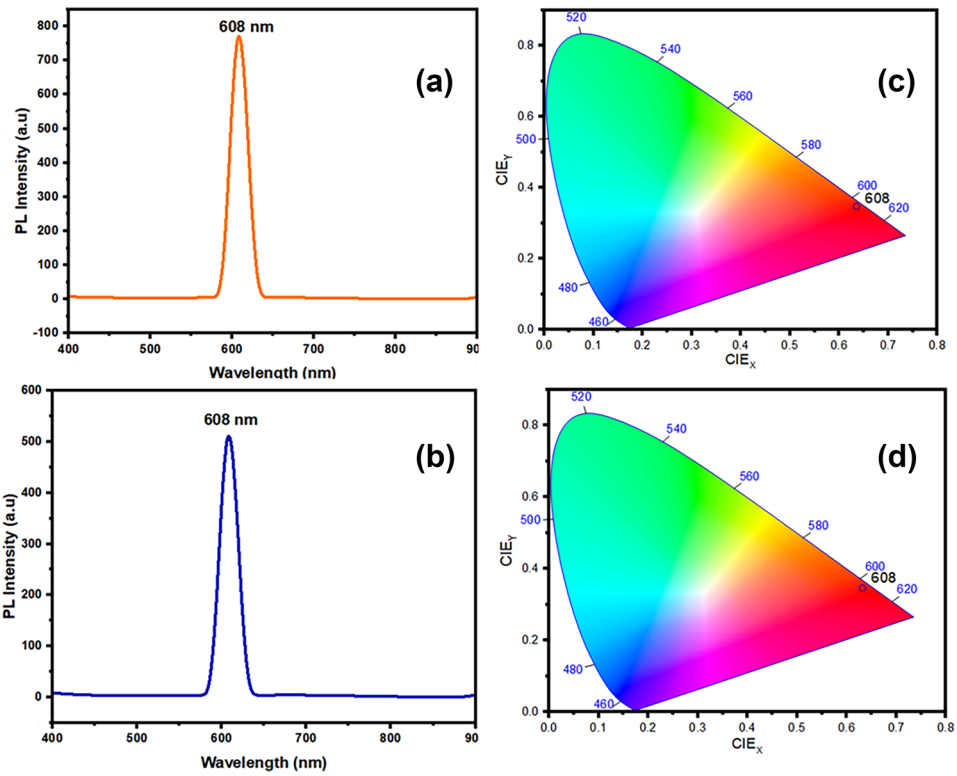

Fig. 8 PL spectra of **a** CdO and **b** Cu–CdO; Chromaticity digram of **c** CdO and **d** Cu–CdO nanoparticles

$$I(t) = I_0 e^{-t/\tau} \tag{4}$$

where I_o is the initial fluorescence intensity, τ is the fluorescence lifetime. The decay rate, k and the decay lifetime τ are related as $k = 1/\tau$.

The fluorescence lifetime for the synthesized CdO was a multi-exponential decay. The photomultiplier tube collected 1.4 million counts in the 60 s. The FWHM of the IRF is 766 ps. The features of the detector and the precise moment of the electrons are what cause this IRF width. The time calibration of the system is 6.955796×10^{-12} s/ch. Figure 9 shows the IRF, the decay, and the fitted multi-exponential curve of CdO and Cu–CdO nanoparticles. The resulting histogram of intensity versus time is the fluorescence decay curve. According to the residual distribution, just less than one photon has been identified per stimulation pulse, which is represented in the inset of Fig. 9. The decay graph of CdO is a tri-exponential fit with three resolved decay components τ_1, τ_2, and τ_3 (4.775007×10^{-11}, 5.662047×10^{-11}, 3.507×10^{-09} s) and their corresponding relative amplitude. A multi-exponential fit is observed, which may be due to the surface defects and heterogeneity of the fluorophore environment [35]. The average lifetime is 52 ps as calculated from Eq. (5) for the CdO sample.

$$\tau_{avg} = \frac{\sum_{i=1}^{n} \alpha_i \tau_i}{\sum_{i=1}^{n} \alpha_i} = \frac{\alpha_1 \tau_1 + \alpha_2 \tau_2 + \alpha_3 \tau_3}{a_1 + a_2 + a_3} \tag{5}$$

where, τ_1, τ_2, τ_3 are the lifetimes of three exponentials and α_1, α_2, α_3 are the relative amplitudes or pre-exponential factors.

The Cu–CdO samples were excited with a pulsed laser at 460 nm (λ_{ex}), and decay measurements were made at 550 nm (λ_{em}). The IRF has an FWHM of 1.87 ns. The decay components, pre-exponential amplitude, and χ^2 values are tabulated in Table 2. The lifetime of Cu–CdO is 40 ps. The lifetime of the CdO is slightly altered by the addition of the Cu-dopant. Since the lifetimes of both CdO and Cu-CdO nanostructures are in the *ps* range, they could be used as inorganic fluorophores in sensing applications.

Antibacterial Analysis

The high rate of resistance of various microbes to most antimicrobial drugs is receiving a lot of attention. Antibiotic-resistant pathogenic microbes pose a serious danger to both human and animal health. Antimicrobial resistance keeps

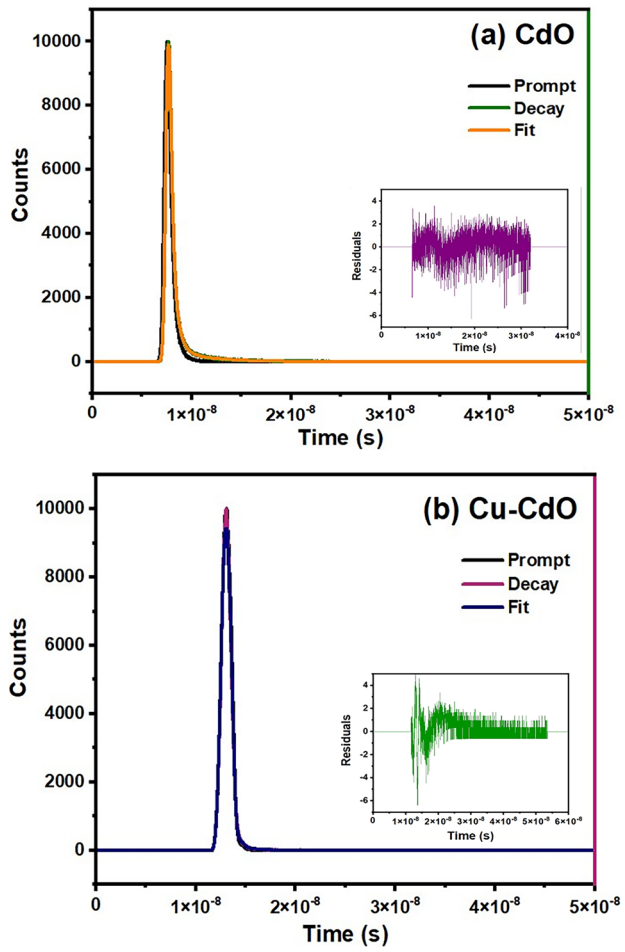

Fig. 9 Fluorescence spectra of **a** CdO and **b** Cu–CdO nanoparticles

rising at an alarming pace due to the extensive use of therapeutic antimicrobial agents. In order to test for antibiotic susceptibility, Mueller–Hinton agar is frequently utilized. Mueller–Hinton agar is employed in clinical diagnosis [36, 37]. The technique of diffusion on agar wells was applied to test the antibacterial effects of the produced nanoparticles against *Micrococcus Luteus* (gram-positive) and *Escherichia Coli* (gram-negative) bacterium at the concentrations of 100, 150, and 200 µg/mL. The antibacterial response of CdO, and Cu–doped CdO nanoparticles are depicted in Fig. 10 and the region of inhibition is listed in Table 3. A well-defined zone forms all around samples because the bacterial strains are vulnerable to the CdO, and Cu–CdO nanoparticles. The extent of the inhibition effect by the nanoparticles is indicated by the zone of inhibition visible on the agar plate. The sample is typically considered to have more potent antibacterial activity if the width of the inhibitory region is wider than 6 mm. Both samples have substantial efficacy against both bacterial strains in the current investigation. The antibacterial activity was more pronounced at higher concentrations. In comparison, Cu–CdO nanoparticles showed a maximum inhibitory region of 24 mm for *Micrococcus Luteus* and 23 mm for *Escherichia Coli*, whereas CdO nanoparticles showed a maximum inhibitory region of 22 mm for Micrococcus Luteus and 18 mm for Escherichia Coli at a 200 µg/mL concentration.

When the nanoparticles interact with the bacteria, they penetrate the bacteria's membrane after reacting with the microbe's functional groups such as –SH, –COOH, and –OH in the cell membrane. The death of bacteria is caused by the inactivation of DNA and cell protein [38]. The CdO nanoparticles have a potent antibacterial effect due to the occurrence of reactive oxygen species (ROS) and the release of Cadmium ions. A higher ROS is associated with increased surface area, particle size, oxygen vacancies, and reactant molecule movement. The hydroxyl (OH^-) radical and superoxide (O_2^-) anion radical found in ROS have the potential to harm DNA and cell membranes. An electrostatic affinity between the nanoparticles and the bacteria causes them to bind together. Bacteria cannot develop in this environment,

Table 2 Fluorescence parameters of CdO and Cu-doped CdO nanoparticles

Sample	Excitation (nm)	Emission (nm)	Lifetime Components τ_i(s)	Pre-exponential amplitude α_i	χ^2	Average Lifetime ($\times 10^{-12}$ s)
CdO	280	339	4.78×10^{-11} 5.66×10^{-11}	6.23 5.35	1.32	52
Cu-CdO	460	550	3.87×10^{-11} 1.29×10^{-09}	0.95 0.03	1.22	40

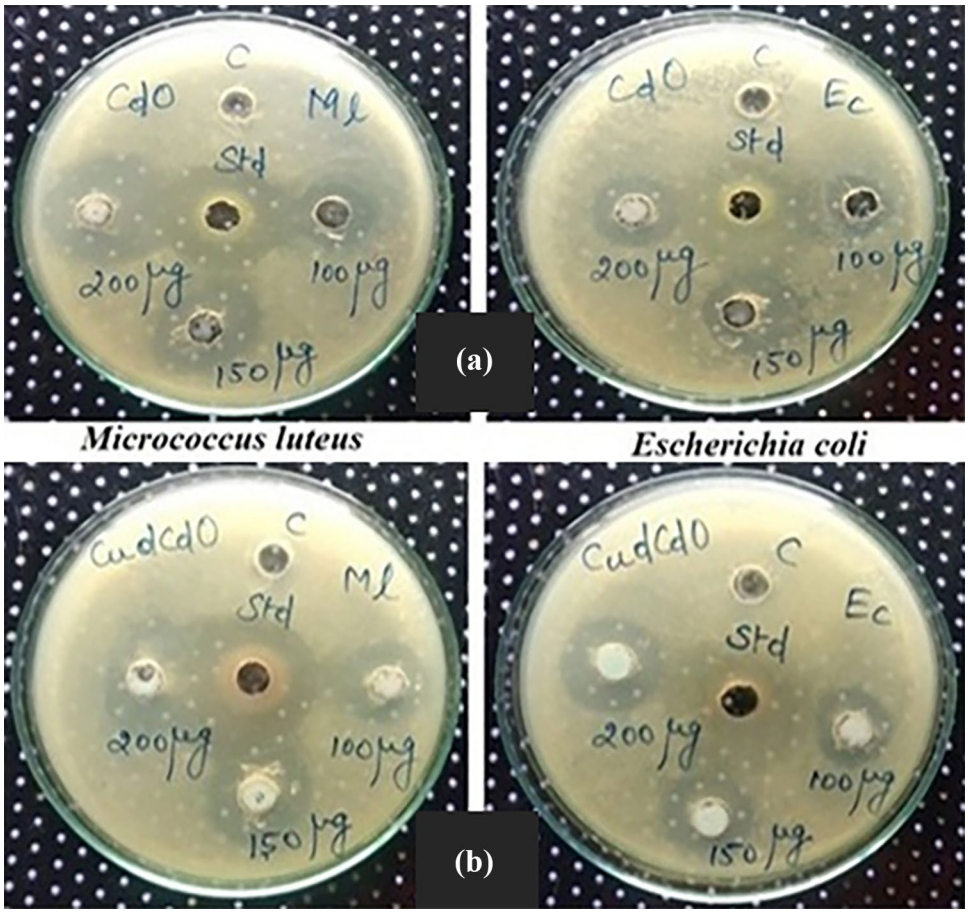

Fig. 10 The antibacterial response of **a** CdO and **b** Cu–CdO nanoparticles

Table 3 Antibacterial efficacy of CdO and Cu-doped CdO nanoparticles

Nanocrystallites	Tested bacteria	Zone of Inhibition (mm)		
		100 µg/mL	150 µg/mL	200 µg/mL
CdO	*Micrococcus luteus*	18	20	22
	Escherichia coli	14	16	18
Cu−CdO	*Micrococcus luteus*	18	22	24
	Escherichia coli	15	17	23

and the generated ROS destroys the cell [39]. According to the findings, the differences in bactericidal action between CdO and Cu–CdO nanoparticles were related to cell capsular disintegration.

Conclusion

In the present study, the co-precipitation process was applied to synthesize CdO and Cu–doped CdO nanoparticles. The samples have been characterized by powder-XRD, FE-SEM, EDX, FT-IR, UV–Vis, PL, fluorescence, and antibacterial effectiveness. According to the powder-XRD study, the CdO and Cu−CdO Nanoparticles are simple cubic in structure, with 54 and 28 nm average grain sizes, respectively. FE-SEM images showed that the synthesized samples are homogenous and porous in nature. The elemental composition has been established via EDX spectra. FT-IR analysis was performed to ascertain the vibrational frequencies of the produced samples. According to UV–Vis spectroscopy, the bandgap values of the CdO and Cu–CdO Nanoparticles were 4.52 and 2.83 eV, respectively. Photoluminescence spectra of the synthesized compounds were obtained by exciting CdO nanoparticles at 300 nm and the characteristic emission is observed in the red region. According to fluorescence spectroscopy, the CdO and Cu–CdO nanoparticles have an average lifetime of 52 and

40 ps, respectively. Since the lifetimes are in picoseconds (*ps*), the produced samples may be used for sensing applications. Agar-well diffusion process was applied to assess the antibacterial performance of the generated nanoparticles against *Micrococcus Luteus* (gram-positive) and *Escherichia coli* (gram-negative) bacterium at variable concentrations. Both the samples showed substantial antibacterial response against both *Micrococcus Luteus* and *Escherichia Coli* at 200 µg/mL concentration. In contrast, Cu–CdO Nanoparticles demonstrated a maximum inhibitory zone of 24 mm for *Micrococcus Luteus* and 23 mm for *Escherichia Coli*, whereas CdO Nanoparticles demonstrated a maximum inhibitory region of 22 mm for *Micrococcus Luteus* and 18 mm for *Escherichia Coli*. According to the findings, CdO and Cu–CdO Nanoparticles could be used as a coating in surgical and hand tools to prevent contamination, particularly from the harmful bacterium.

Author Contributions J. Christina Rhoda: Conceptualization, Data Curation, Formal Analysis and Investigation. S. Chellammal: Methodology, Supervision, Validation. Helen Merina Albert: Writing- Original Draft Preparation, Visualization. K. Ravichandran: Methodology, Validation, Resources. C.Alosious Gonsago: Writing- Review and Editing, Resources and Software.

Availability of Data and Materials The datasets generated during and/or analyzed during the current study are available from the corresponding author on reasonable request.

Declarations

Ethical Approval This article does not contain any studies with human participants or animals performed by any of the authors.

Competing Interests The authors declare that no funds, grants, or other support were received during the preparation of this manuscript.

References

1. Yathisha RO, Arthoba Nayaka Y, Vidyasagar CC (2016) Microwave combustion synthesis of hexagonal prism shaped ZnO nanoparticles and effect of Cr on structural, optical and electrical properties of ZnO nanoparticles. Mater Chem Phys 181:167–175. https://doi.org/10.1016/j.matchemphys.2016.06.046
2. Valentina M, Luisana DC, Stephen GJS, Simona O, Magda B, Anna C, Pierluigi R, Yuri V, Adriele M (2018) Silver nanoparticles as a medical device in healthcare settings: a five-step approach for candidate screening of coating agents. Roy Soc Open Sci 5:171113. https://doi.org/10.1098/rsos.171113
3. Chulasak K, Punsawad C, Rattanakit P (2022) Silver nanoparticles synthesized from Launaea sarmentosa extract: synthesis, characterization, and antimalarial activity. Nanotech Environ Eng 7:491–501. https://doi.org/10.1007/s41204-022-00239-z
4. Zhang Y, Wang Z, Yu-Cheng Chen (2021) Biological tunable photonics: Emerging optoelectronic applications manipulated by living biomaterials. Prog Quant Electron 80:100361. https://doi.org/10.1016/j.pquantelec.2021.100361
5. Sinha SN, Paul D (2015) Phytosynthesis of Silver Nanoparticles Using Andrographis paniculata Leaf Extract and Evaluation of Their Antibacterial Activities. Spect Lett 48:600–604. https://doi.org/10.1080/00387010.2014.938756
6. Helmly BC, Lynch WE, Nivens DA (2007) Preparation and Spectroscopic Characterization of MoS_2 and $MoSe_2$ Nanoparticles. Spect Lett 40:483–492. https://doi.org/10.1080/00387010701295984
7. Talapin DV, Lee JS, Kovalenko MV, Shevchenko EV (2010) Prospects of Colloidal Nanocrystals for Electronic and Optoelectronic Applications. Chem Rev 110:389–458. https://doi.org/10.1021/cr900137k
8. Hone FG, Tegegne NA, Dejene FB, Andoshe DM (2021). Nanofiber CdO thin films prepared from ethanolamine complexing agent by solution growth method. Optik 243:167402. https://doi.org/10.1016/j.ijleo.2021.167402
9. Munshi A, Prakash T et al (2022) Comparative investigation of physicochemical properties of cadmium oxide nanoparticles. Ceram Internat 48:4134–4140. https://doi.org/10.1016/j.ceramint.2021.10.204
10. Kannan SK, Thirunavukkarasu P et al (2022) Influence of In Doping on Physical Properties of Co-precipitation Synthesized CdO Nanoparticles and Fabrication of p-Si/n-$CdIn_2O_4$ Junction Diodes for Enhanced Photodetection Applications. J Electron Mater 51:1759–1777. https://doi.org/10.1007/s11664-021-09427-0
11. Ghoroghchian PP, Therien MJ, Hammer DA (2009) In vivo fluorescence imaging: a personal perspective. WIREs Nanomed Nanobiotechnol 1:156–167. https://doi.org/10.1002/wnan.7
12. Pandey S, Bodas D (2020) High-quality quantum dots for multiplexed bioimaging: A critical review Adv Coll Interf Sci 278:102137. https://doi.org/10.1016/j.cis.2020.102137
13. Millar DP (1996) Time-resolved fluorescence spectroscopy. Curr Opin Struct Bio 6:637–642. https://doi.org/10.1016/S0959-440X(96)80030-3
14. Labiadh H, Hidouri S (2017) ZnS quantum dots and their derivatives: Overview on identity, synthesis and challenge into surface modifications for restricted applications. J King Saud Univ Sci 29:444–450. https://doi.org/10.1016/j.jksus.2016.12.001
15. Belkhaoui C, Mzabi N, Smaoui H (2019) Investigations on structural, optical and dielectric properties of Mn doped ZnO nanoparticles synthesized by co-precipitation method. Mater Res Bull 111:70–79. https://doi.org/10.1016/j.materresbull.2018.11.006
16. Yathisha RO, Arthoba Nayaka Y, Manjunatha P, Purushothama HT, Vinay MM, Basavarajappa KV (2019) Study on the effect of Zn2+ doping on optical and electrical properties of CuO nanoparticles. Physica E: Low-dimen Syst Nanostruct 108:257–268. https://doi.org/10.1016/j.physe.2018.12.021
17. Sayas MR, Fadavieslam MR (2020) Influence of deposition conditions on structural, electrical, and optical properties of cadmium oxide thin films deposited using the spray pyrolysis technique. J Mater Sci Mater Electron 31:18320–18335. https://doi.org/10.1007/s10854-020-04275-w
18. Chaure S (2017) Synthesis and characterization of vertically aligned cadmium oxide nanowire array. J Mater Sci Mater Electron 28:1832–1836. https://doi.org/10.1007/s10854-016-5733-5
19. Benhaliliba M, Benouis CE et al (2012) Luminescence and physical properties of copper doped CdO derived nanostructures. J Lumin 132:2653–2658. https://doi.org/10.1016/j.jlumin.2012.03.044
20. Nasar S, Murtaza G et al (2019) Environmentally Benign and Economical Phytofabrication of Silver Nanoparticles Using Juglans regia Leaf Extract for Antibacterial Study. J Electron Mater 48:3562–3569. https://doi.org/10.1007/s11664-019-07109-6
21. Manjunatha KB, Bhat RS et al (2021) Antimicrobial and Nonlinear Optical Studies of Copper Oxide Nanoparticles. J Electron Mater 50:3415–3421. https://doi.org/10.1007/s11664-021-08838-3
22. Robert Xavier A, Ravichandran AT et al (2016) (2016) Sm doping effect on structural, morphological, luminescence and antibacterial activity of CdO nanoparticles. J Mater Sci Mater Electron 27:11182–11187. https://doi.org/10.1007/s10854-016-5237-3
23. Lohitha T, Albert HM (2023) Biosynthesis of pure and MnSO4 (II) doped CeO2 nanoparticles: Electrochemical studies and its

antibacterial activity. Mater Tod Proceed. https://doi.org/10.1016/j.matpr.2023.02.239
24. Cullity BD, Stock SR (1978) Elements of X-ray diffraction. Addison-Wesley, Philippines
25. Mohanraj K, Balasubramanian D, Chandrasekaran J, Chandra Bose A (2016) Synthesis and characterizations of Ag-doped CdO nanoparticles for P-N junction diode application. Mater Sci Semicond Process 79:74–91. https://doi.org/10.1016/j.mssp.2018.02.006
26. Albert HM, Lohitha T, Alagesan K, Alosious Gonsago C, Vinita V (2021) Performance of ZnSO4 doped CeO2 nanoparticles and their antibacterial mechanism. Mater Tod Proceed 47:1030–1034. https://doi.org/10.1016/j.matpr.2021.06.124
27. Gonsago CA, Albert HM, Malliga P, Joseph Arul Pragasam A (2012) Growth and Characterization of Pure and Thiourea Doped L-Histidine Single Crystals. Mater Manuf Process 27:355–359. https://doi.org/10.1080/10426914.2011.585495
28. Zhao C, Zhang Y, Wang CC, Hou M, Li A (2019) Recent progress in instrumental techniques for architectural heritage materials. Herit Sci 7:36. https://doi.org/10.1186/s40494-019-0280-z
29. Tugrul N, Bardakci M, Ozturk E (2015) Synthesis of hydrophobic nanostructured zinc borate from zinc carbonate, and characterization of the product. Res Chem Intermed 41:4395–4403. https://doi.org/10.1007/s11164-014-1538-4
30. Rautela A, Rani J, Debnath D (2019) Green synthesis of silver nanoparticles from Tectona grandis seed extract: Characterization and mechanism of antimicrobial action on different microorganisms. J Anal Sci Techol 10. https://doi.org/10.1186/s40543-018-0163-z
31. Kumar V, Sharma DK, Sharma KP, Agarwal S, Bansal MK, Dwivedi DH (2016) Structural, optical and electrical characterization of nanocrystalline CdO films for device applications. Optik 127:4254–4257. https://doi.org/10.1016/j.ijleo.2016.01.186
32. He H, Wu C, Saqib M et al (2023) Single-molecule fluorescence methods for protein biomarker analysis. Anal Bioanal Chem. https://doi.org/10.1007/s00216-022-04502-9
33. Becker W, Bergmann A, Hink MA, König K, Benndorf K, Biskup C (2004) Fluorescence lifetime imaging by time-correlated single-photon counting. Micro Res Tech 63:58–66. https://doi.org/10.1002/jemt.10421
34. Kahane SV, Sasikala R, Vishwanadh B, Sudarsan V, Mahamuni S (2013) CdO–CdS nanocomposites with enhanced photocatalytic activity for hydrogen generation from water. Internat J Hydro Ener 38:15012–15018. https://doi.org/10.1016/j.ijhydene.2013.09.077
35. Chen J, Lv J, Liu X, Lin J, Chen X (2023) A study on theoretical models for investigating time-resolved photoluminescence in halide perovskites. Phys Chem Chem Phys 25:7574–7588. https://doi.org/10.1039/D2CP05723A
36. Roy K, Sarkar CK, Ghosh CK (2015) Plant-mediated synthesis of silver nanoparticles using parsley (petroselinum) leaf extract: spectral analysis of the particles and antibacterial study. Appl Nanosci 5:945–951. https://doi.org/10.1007/s13204-014-0393-3
37. Sathishkumar G, Gopinath C, Karpagam K, Hemamalini V, Premkumar K, Sivaramakrishnan S (2012) Phyto-synthesis of silver nano scale particles using Morinda citrifolia L. and its inhibitory activity against human pathogens. Coll Surf B 95:235–240. https://doi.org/10.1016/j.colsurfb.2012.03.001
38. Kalaiarasi S, Jose M (2017) Streptomycin loaded TiO2 nanoparticles: preparation, characterization and antibacterial applications. J Nanostruct Chem 7:47–53. https://doi.org/10.1007/s40097-016-0213-2
39. Ye L, Cao Z, Liu X, Cui Z, Li Z, Liang Y, Zhu S, Wu S (2022) Noble metal-based nanomaterials as antibacterial agents. J Alloy Compd 904:164091. https://doi.org/10.1016/j.jallcom.2022.164091